University of Tennessee, Knoxville
TRACE: Tennessee Research and Creative Exchange

Chancellor's Honors Program Projects

Supervised Undergraduate Student Research and Creative Work

Spring 4-2005

Modeling and Docking Studies of Anti-Anyloid Antibodies WOL and WOZ

Nathanael Alan Tanner
University of Tennessee - Knoxville

Follow this and additional works at: https://trace.tennessee.edu/utk_chanhonoproj

Recommended Citation

Tanner, Nathanael Alan, "Modeling and Docking Studies of Anti-Anyloid Antibodies WOL and WOZ" (2005). *Chancellor's Honors Program Projects.*
https://trace.tennessee.edu/utk_chanhonoproj/920

This is brought to you for free and open access by the Supervised Undergraduate Student Research and Creative Work at TRACE: Tennessee Research and Creative Exchange. It has been accepted for inclusion in Chancellor's Honors Program Projects by an authorized administrator of TRACE: Tennessee Research and Creative Exchange. For more information, please contact trace@utk.edu.

Modeling and Docking Studies of anti-Amyloid Antibodies WO1 and WO2

Nathan Tanner
Dealwis Lab, University of Tennessee Department of Biochemistry, Cellular and Molecular Biology

Submitted for Completion of the Senior Honors Project, University of Tennessee Honors Program

5 April 2005

Abstract

WO1 and WO2 are conformation-specific monoclonal IgMs that bind the fibril state of the amyloid Aβ peptide (1-40), as well as amyloid fibrils of other disease-related proteins. Significantly, the antibodies (Abs) do not bind the soluble, monomeric state of Aβ (1-40) or the precursor form of other amyloids. The Abs have been sequenced and analyzed to study the role of the unique and unusual residues in WO1 and WO2. Three-dimensional models of the Fv fragments of WO1 and WO2 were generated with Web Antibody Modeling. A left-handed, six-rung structural model of the Aβ amyloid core was evaluated by docking it with the Fv models of WO1 and WO2. The results predict binding of WO1 and WO2 to Aβ *via* hydrogen bonds and ionic pairing between the CDRs and the protofilament face consisting of residues 23-27. WO1 and WO2 bind the model in similar configurations; binding to WO2 is predicted to rely less on ion pairing. The results support the Aβ model. Binding of WO1 experimentally determined to be sensitive to salt and pH conditions, suggesting electrostatic interactions are important for binding; this result supports the proposed docking model for WO1.

Introduction

The aggregation of normally soluble proteins into insoluble, unbranched fibrils is the underlying pathology of a family of diseases known as the amyloidoses.[1] The hallmark event in amyloidogenesis is a change in the secondary and/or tertiary structure of a normal, soluble protein, rendering it prone to self-assembly into highly ordered para-crystalline arrays, or fibrils. More than 20 proteins have been clinically identified as precursors of amyloid fibrils *in vivo*. These include the amyloid precursor protein (APP), Islet amyloid polypeptide (IAPP), α-synuclein, transthyretin (TTR), immunoglobulin light chain (LC), polyglutamine-repeats, and prion proteins, that are associated with diseases such as Alzheimer's,[2-4] type II diabetes,[5,6] Parkinson's disease,[7-9] familial polyneuropathy,[10] light chain associated (AL) amyloidosis,[11-13] Huntington's disease,[4,14] and the spongiform encephalopathies.[15] By understanding the three-dimensional structure of such fibrils, we might design novel agents for detection and/or therapeutics. It is notoriously difficult to extract structural information directly from amyloid fibrils, which are insoluble and non-crystalline, so a great deal of study has gone into fiber diffraction studies,[16-18] mutation studies,[19] microscopy,[17,20,21] proteolysis,[22,23] ESR,[24,25] NMR,[24,26] SANS,[27] and deuterium exchange[28-31] in an ongoing attempt to elucidate the molecular structure of the amyloid Aβ fibrils associated with Alzheimer's disease.

There is no consensus model for Aβ structure, but most models incorporate a cross-beta secondary structure. The cross-beta structure (in which the fibril axis is perpendicular to the chain direction) of Aβ models is derived from the 4.75 Å meridional reflection in fiber diffraction studies. A stacked, parallel beta-sheet arrangement is suggested by Burkoth, Benzinger, and others,[24,27,32] while a pair of concentric cylinders was proposed by the late M. F. Perutz , *et al.*[33] An anti-parallel or stacked-hairpin beta-sheet arrangement is suggested by Callaway and others.[34-37]

One recent model of the Aβ protofilament features a trigonal prism of stacked, parallel Aβ(15-36) polypeptides; the model is visible in **Figure 5**. This model is consistent with hydrogen-deuterium exchange, limited proteolysis, solid-state NMR, EPR, and proline-scanning mutagenesis data.[38] The model remains stable and gains order during molecular dynamics simulations, supporting the viability of the trigonal prism model. The proposed fibril model (of 6 protofilaments) that accompanies the protofilament model appears to be consistent with electron microscopy. Hence, it may serve as a starting model for simulating Aβ-antibody interactions.

Each unique monoclonal antibody binds specifically to a particular antigen via an antigen binding domain of the Ab, the Fab domain, recognizing a specific antigenic region, the epitope. They can thus be used to detect and diagnose certain conditions, such as disease or drug use. They are also useful as therapeutic agents with precise targeting and correspondingly reduced side effects. The monoclonal antibodies WO1 and WO2 appear to recognize a common conformational epitope shared by several different types of amyloid fibrils, with little dependence on amino acid sequence.[39] The two bind the same antigen with similar affinities for the Aβ fibril.[39] This result opens the door to targeting whole classes of amyloid fibrils for detection and therapy.[40] The success of antibody modeling algorithms at predicting crystal structures of antibody variable regions[41] encouraged us to use computed models of WO1 and WO2 Fvs for docking simulations, albeit cautiously.

The program Autodock predicts the interaction of ligands with macromolecular targets. Autodock is flexible enough to accept the hexamer protofilament model as an input. Since WO1 and WO2 bind to Aβ amyloid, we hypothesized that a model of the Aβ protofilament would, if correct, dock predictably to a model of the variable regions of WO1 and WO2. Here is presented the configuration predicted by Autodock3 for the binding of the Fvs of antibodies WO1 and WO2

to a model of Aβ protofilament. Also are comparisons of the sequences of WO1 and WO2 variable regions to each other and to sequences in the database and experimental data that supports the predicted model of WO1-Aβ binding with respect to salt-dependence.

Methods

Sequence analysis- The nucleotide sequences of WO1 and WO2 were obtained by cloning and confirmed by multiple cloning using high fidelity polymerases, and further confirmed by extended N-terminal amino acid sequence from analysis of the protein.[42] Initial alignments were performed using Molecular Operating Environment (MOE™[43]), with Ab sequences obtained from the Protein Data Bank[44,45]. An extensive alignment was done using the Kabat sequence database testing program[46]. BLASTP analysis[47] was run on the WO1 and WO2 variable light chains using the Non-Redundant Protein Database at the San Diego Supercomputer Center. Canonical classes are based on Chothia nomenclature[48] and numbering scheme is that of Kabat[49].

Electrostatic Analysis - Electrostatic surfaces were calculated using DelPhi, a part of the InsightII® graphical software package. Models were displayed and manipulated with InsightII® and all computational work done on a Silicon Graphics computer system.

Model Generation- Models of WO1 and WO2 variable regions (Fv) were generated using the Web Antibody Modeling algorithm, WAM.[41] WAM is an improvement on the AbM program [50-53] with greater capability in modeling the highly variable H3 loop through a combination of knowledge-based and *ab initio* methods[41] . The WAM algorithm has a record of producing models that are 1.0-2.8 Å RMSD from observed structures for the (notoriously low homology) heavy chain CDR3, and better than that for the canonical loops (typically 1.0-2.5 Å RMSD).

Docking – preparation. With Anna Gardberg in the Dealwis lab, docking simulations were performed using Autodock and a Silicon Graphics workstation. Control calculations performed

with a protein-peptide complex and a protein-ligand complex of known structure showed that the charges assigned from forcefield calculations performed by AutoDockTools yielded less accurate results than those assigned by AMBER forcefield calculations[54,55] performed by InsightII.[56] We report here the procedure that we used to assign such charges. A PDB file of the Aβ 1-40 hexameric protofilament model after molecular dynamics simulations ("Aβ6 model", which models residues Gln15 through Val36)[38] was kindly provided by Juntao Guo and Ying Xu. The atom names were standardized and hydrogen atoms added in riding positions *via* Refmac5.[57,58] After capping the termini of each chain with neutral end groups, the InsightII program calculated partial charges for each atom (including H's) in the Aβ6 model *via* the AMBER force field. Calculating the summed formal and partial charges for the Aβ6 model verified that the model is electrically neutral.

Docking – computation. Autodock-style PDBQ files were prepared files with *mol2topdbq* and *mol2topdbqs*, awk-based utilities packaged with Autodock3.[59] For purposes of solvation calculation, we designated the Fab models the proteins and the Aβ6 model the ligand. Despite the thermodynamic importance of side-chain motion,[60] neither the Fvs nor the Aβ6 model were permitted any torsional freedom; the Autodock package does not permit the side chains of the protein to move, and the Autotors utility for designating rotatable bonds in the ligand allows a maximum of 32, not nearly sufficient for a "ligand" the size of the Aβ6 model, which contains 2040 atoms. Grid parameter files were generated *via mkgpf3* (a script which comes packaged with Autodock3) and adjusted to compensate for the large volume required for the interaction of the Fab's complementarity determining region (CDR) with the Aβ6 model. The *npts* parameter, which controls the number of points in the docking grid, was adjusted to "120 120 120", the spacing between points was increased to 0.55 Å, and the center of the computational volume was moved.

The final gridded regions encompassed the CDR of the Fv (as well as all of the heavy chain and most of the light chain of the model for WO1, and all save the C-termini for WO2) and the starting position of the Aβ6 model, with room for rotation and translation. Grid generation was performed with Autogrid3.

Docking parameter files were prepared with *mkdpf3* and adjusted by hand. The *qstep* parameter was changed to 180 for more initial rotational freedom. The initial *ga_pop_size* of 10 was insufficient for meaningful clustering results, so that parameter was changed to 50.

Contact analysis. Contacts between the Fv models and the Aβ6 model in the predicted docking complexes were analyzed with Tadeusz Skarzynski's program CONTACT.[58] Docking clusters and configurations were examined in Pymol,[61] with residue charge surfaces visualized. Electrostatic surface plots for publication were generated by the DelPhi module of InsightII.[56] Angles between solutions were computed by calculating the average direction vector along the protofilament axis for each solution and taking the inverse cosine of the dot-product of direction vectors.

Salt Effects on Binding WO1. Binding of the WO1 antibody to Aβ fibrils was tested under various salt and pH conditions, experiments conducted by Israel Huff and data communicated. A buffer concentration of 5mM was used throughout: HEPES at pH 7.5 with 1) no salt, 2) 150 mM NaCl, 3) 600 mM NaCl, 4) 150 mM KCl, and 5) 75 mM Na_2HPO_4 comprised the salt-effects experiments; 150 mM NaCl with 6) citric acid pH 3.0, 7) citric acid pH 5.8, 8) PIPES at pH 5.8, 9) PIPES at pH 7.4, 10) Bicine at pH 7.4, 11) Bicine at pH 8.5, 12) CHES at pH 8.5, and 13) CHES at pH 10.0 comprised the pH-effects experiments.

All buffer compounds except citric acid were ordered from Calbiochem. HEPES has low ionic strength, so it should not interfere greatly with comparing the different salts. Na_2HPO_4 has

roughly double the ionic strength of the other 2 salts so it was used at half the concentration for a balanced comparison. The salt-effects experiments were buffered to pH 7.5, near physiological pH conditions. The pH effect experiments contained 150 mM NaCl to provide approximate physiological ionic strength conditions. Four different salts were tested at comparable ionic strengths to determine if the particular salt present in the buffer has a significant impact on antibody binding. The four chosen were 1xPBS, NaCl, KCl, and $NaPO_4$. 1xPBS is the standard buffer used in the binding experiments. The other three salts were chosen to compare two different anions and cations.

RESULTS

Sequence analysis. Comparison of WO1 to WO2. The WO1 and WO2 Fv residue sequences were initially compared to one another, then compared with sequences from the Kabat database to search for anomalies, unique features, or homologies to other antibodies. An alignment of the CDRs is shown in Figure 1. The light chain variable regions share 66% identity (80% similarity) and the heavy chain variable regions share 82% identity (85% similarity). While both sequences are rich in hydrogen bonding residues, WO1 V_L has a greater proportion of Asn and Gln residues (10.7% WO1 vs. 4.9% WO2) and of (charged) Asp, Glu, Arg, and Lys residues (13.3% vs. 11.5%), while the WO2 light chain is richer in Ser residues (13.2% for WO1 V_L, 20.3% for WO2 V_L). Of the eleven additional serine residues in WO2's light chain variable region, nine are in the CDRs; their counterparts in WO1 are Gly, Asn (3), His, a deletion, Lys, Asp, and Thr. The number of positively and negatively charged residues in the V_L region is similar; the number of charged residues in the V_H is identical. The WO1 and WO2 heavy chain variable regions are more similar in overall sequence, but WO2 is richer in serine residues (WO1: 12.8%, WO2: 14.9%). Only one of the additional serine residues is at a CDR, and it replaces a (similar) threonine residue.

Overall charge composition of the Fv fragments is very similar, with isoelectric points (pIs) of the variable regions calculated to be: WO1 V_H 7.3, V_L 8.7, WO2 V_H 7.2, and V_L 8.7. The CDRs of the light and heavy chains are rich in hydrogen-bonding residues relative to anti-lysozyme and germline antibodies, suggesting that hydrogen bonding plays a role in amyloid-recognition. The compositions of CDR1 and CDR2 feature a much higher composition of hydroxyl residues in WO2 than in WO1. This disproportion could feature in any antigen binding differences or trends between the two Abs. CDR3 of the heavy chain shows high variability, so comparisons are difficult, but the three-charge region R98, D99, D100 in WO1 heavy-chain CDR3 is striking, this being the only chain with three-charge region. (WO2 has RRL here). **Figure 1** displays the sequence comparison for the CDRs.

a)

VL CDR1	24	25	26	27	28	29	30	31	31a	32	33	34
WO1	R	A	S	G	N	I	H	N	-	Y	L	A
WO2	T	A	S	S	S	V	S	S	S	Y	L	H
α-Lyso	R	A	S	Q	N	I	S,H	N	N	-	L	H,A
Germ.	R,K	S,A	S	Q	S,N	I	nh*	nh	S	nh	L	nh
Kappa	R,K	A,T	S	Q	nh	V,I	nh	S,T	-	nh	L	nh

CDR2,3	50	51	52	53	54	55	56	89	90	91	92	93	94	95	96	97
WO1	N	A	K	T	L	A	D	Q	H	F	W	S	T	P	Y	T
WO2	S	T	S	N	L	A	S	L	Q	Y	H	R	S	P	Y	T
α-Lyso	Y	T	T,S	Q,T	S,L	nh	D,S	Q	Q	F,Y	nh	S	-	P	R,L	T
Germ	nh	A,V	S,A	nh	R,L	D,E	S	nh	Q	nh	S	nh	nh	P	R	T
Kappa	nh	A	S	nh	R,L	nh	S	Q	Q	S,Y	nh	S,D	nh	P	R,L	T

b)

VH CDR1	26	27	28	29	30	31	32	33	34	35
WO1	G	Y	T	F	T	E	Y	T	M	H
WO2	G	Y	S	F	T	G	Y	T	M	N
α-Lyso	G	Y	T,S	F	T	T	Y	W	I,V	E,S
Germ	G	F	T	F	T	D	Y	Y	M	S,H
Kappa	G	F,Y	T	F	T	D	Y	Y	I,M	H,K

CDR2	50	51	52	53	54	55	56	57	58
WO1	G	I	N	P	N	N	G	T	S
WO2	L	I	N	P	Y	N	G	T	S
α-Lys	E	I	L	P	G	S	nh	T	Y,D
Germ	F	I	R	nh	nh	nh	nh	T	E,K
Kappa	nh	I	nh	P	nh	nh	G,S	T	nh

Figure 1:
CDR composition of a) V_Ls and b) V_Hs compared with those of anti-lysozyme, germline, and kappa-light-chain antibodies. CDR3 for V_H not shown as this region has high variability. **nh* signifies no homology

Light Chain. A preliminary sequence alignment was performed using a database of various antibody sequences, including subsets of anti-lysozyme Ab chains and germline Ab chains. The results showed a high degree of homology between the chains on the whole, with several residues noted as distinctive. (**Table I**). In WO1's light chain CDRs, there are charged residues occupy positions occupied by hydroxyl residues in WO2 and the comparison sequences: Arg24, Lys52, and Asp56. Similarly, theWO2-unique charged residue Arg93 replaces a hydroxyl residue in WO1 and the other comparison sequences. In other words, the unique residues of WO1 are not conserved in WO2, and *vice versa.*

Light Chain Residue WO1 WO2	**Equivalents**	**Residue exhibited by chains with non-identity**
Lys42 Ser43	No	None charged, only Gly, Gln, Tyr
Lys52 Ser53	Lys only in WO1	No charged, 95% Tyr or Ser
Asp56 Ser57	Asp in WO1 and (AL)	99% Pro, (G) have Thr/Ser
Lys74 Thr75	Lys only inWO1	100% Glu/Asp, (G) has Thr

Table I: Light chain-unique residues and comparison for WO1 residues that are less than 10% homologous in the initial alignment tests. The alignment was done with specific interest in the anti-lysozyme Abs as well as germline Abs, and any residues here are noted if appearing in either chain. The residue is listed with its location, as well as the residues that were most commonly shared throughout the other Ab sequences. The equivalent residue from WO2 is also included for comparison. Codes: antilysozyme (AL), germline (G).

Light Chain Kabat Alignment. A more extensive alignment was done using the Kabat sequence database testing program. The WO1 V_H and V_L sequences were compared to the database of 2707 light chains and 3471 heavy chains. The chain of interest was displayed against a code of typical residues by name or property, indicating what residue or what type (hydrophobic, acidic, basic, hydroxyl, etc.) of residue occurs at each position in the majority of the comparison sequences. The unique (defined as: occurring in less than 1% of the chains at a certain position) residues Lys42 and Lys74 had no consensus within the database. Lys52, however, was a hydroxyl residue in the majority of the 2701 chains. None of the WO2-unique charged or hydroxyl residues showed any incongruity.

Heavy Chain. Through the preliminary alignment including the anti-lysozyme, germline, and kappa-light chain sequences, the following were noted as distinctive in the WO1/WO2 heavy chain:

Heavy Chain Residue WO1 WO2	**Equivalents**	**Residue exhibited by chains with non-identity**
Lys63 Lys63	WO1/WO2, (G)	No other charged residues
Lys65 Lys65	WO1/WO2, (G), (AL)	100% Val, Leu, or Phe
Lys67 Lys67	WO1/WO2, (G), (AL)	100% Gly, Ser, Asp
Asp73 Asp73	WO1/WO2, (G), (AL)	Mostly Asp/Glu
Lys74 Lys74	WO1/WO2, (G)	99% Asp/Glu
Arg84 Leu84	Arg only in WO1	Non-consensus, but no other charged

Table II: Heavy chain unique residues and comparison. The residues displaying less than 10% homology in the initial alignment tests are included here. Any germline or anti-lysozyme Ab commonalities are noted, as well as the residues displayed in the chains which are not homologous to the WO1/WO2 heavy chains. Codes: antilysozyme (AL), germline (G).

Similar to the light chain results, the most striking disparities between WO1/WO2 and comparison sequences occur with charged residues, here Lys63, Lys65, Lys67, Lys74, Asp73 (both WO1 and WO2) and Arg84 (WO1 only).

Kabat Alignment. Again, the Kabat alignment was performed to determine uniqueness or find other distinct residues. None of the above charged residues were found unique, and the typical equivalent had no consensus. The only significant discrepancy was the Asn44 of the WO2 heavy chain. The Asn residue found at this site is found in only 13 examples, 0.326% of the database. Typically, a Ser residue is at this position.

Electrostatic surface potentials for WO1 and WO2. WO1 and WO2 Fvs display regions of significant charge density, indicated in the electrostatic potential map in **Figure 2**. Though the pIs of the WO1 and WO2 Fvs are nearly neutral, they clearly have highly charged regions. The presence and distribution of these charged segments indicates a possible role of charge interactions in antigen binding. The line of positively charged residues on each of the light-chains suggests a template for hydrogen bonding and salt bridges.

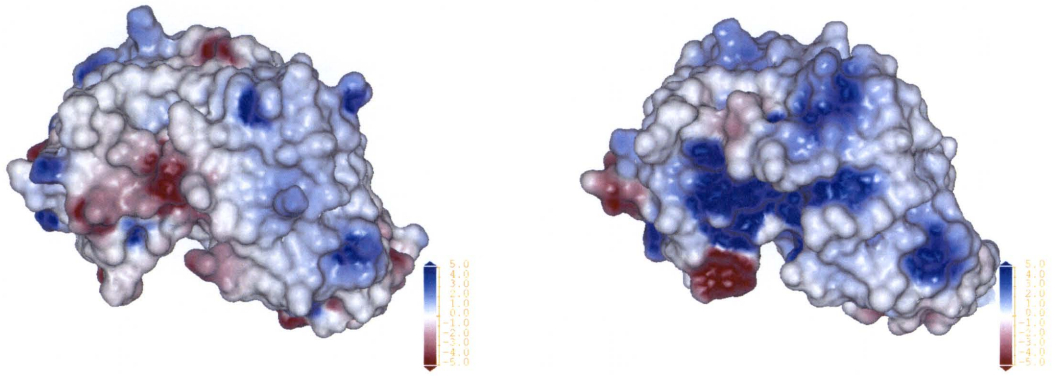

Figure 2. Electrostatic surfaces for WO1 (left) and WO2 (right) Fv models. The viewer faces the CDRs. In each image, the heavy chain fragment is on the left.

Fv Models. Of the WO1 light chain's unique lysine residues (42, 52, and 74), only Lys52 is at the CDR and plays a role in docking. Lys74 and Lys42 are on the framework; Lys42 sits near the heavy-light interface. The heavy chain's unique residues (common to WO1 and WO2), Lys63, Lys65, Lys67, Asp73, and Lys74, likewise do not occupy the CDR, and play no part in the binding predicted by these models. WO1 light-chain Asp56 (unique to WO1 and anti-lysozyme Abs) does play a role, however.

Electrostatic Surface Potentials for Aβ6. The most striking features of the Aβ6 model are the bands of charged residues aligned along the stacking axis, shown in **Figure 3**. These charged bands are a consequence of the in-register parallel-stacking of the model. Labeling the protofilament face containing residues 17-22 "A", 23-27 "B", and 28-36 "C" (Aβ 1-40 numbering basis), we see that faces A and C display exposed hydrophobic residues.

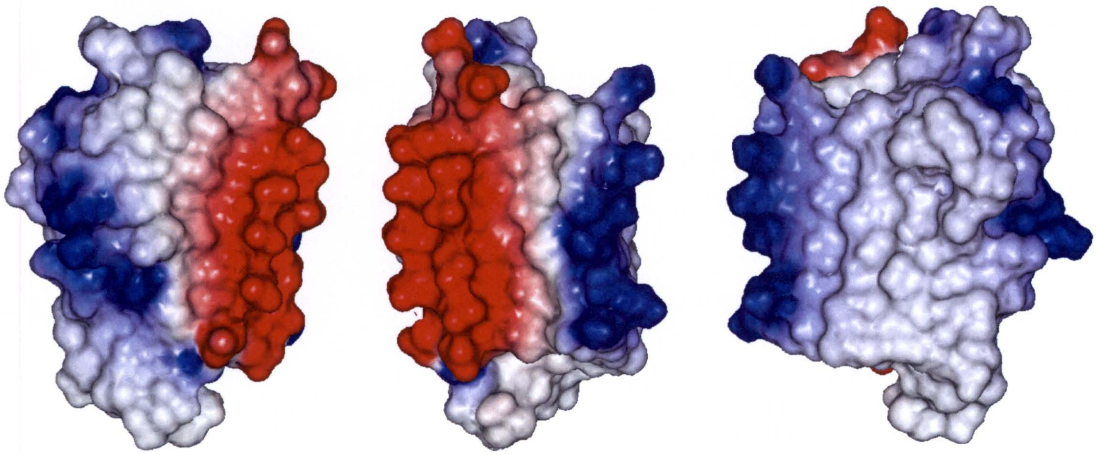

Figure 3. Electrostatic surfaces for the A, B, and C faces of the Aβ6 protofilament model. The line of Glu22 and Asp23 residues (shown in red) at the corner of the A and B faces is particularly striking.

Protofilament Packing model. **Figure 4** shows a more detailed three-dimensional view of the 6-protofilament packing model suggested by Guo, Wetzel, and Xu.[38] Each unique protofilament face is exposed twice on the outside of the fibril.

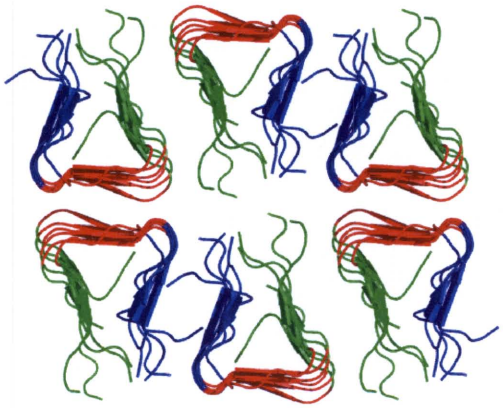

Figure 4. A more detailed (but still schematic) three-dimensional view of the 6-protofilament packing model suggested by Guo, Wetzel, and Xu.[38] Each unique protofilament face is exposed twice on the outside of the fibril. Color scheme: A-face, blue; B-face, red; C-face, green.

Docking. WO1-Aβ6. AutoDock3 predicted 50 binding configurations for WO1- Aβ6. Both Fvs were treated as rigid bodies. For WO1- Aβ6, Autodock3 found 41 distinct conformational clusters (using an RMSD-tolerance of 1.0 Å), of which 8 contained more than one member. The variation in

energy from the best to the worst solution was 7.0 kcal/mol. Although there was one cluster of two solutions in the top 7, more intriguing is a collection of related clusters beginning at the 8th-ranked solution. In total, 21 solutions have the B face of the Aβ6 protofilament model at the light-chain CDR, with some overlap onto heavy chain CDR. Some are offset by one, two, or three monomers (i.e., the stack of six Aβ monomers is shifted along the stacking axis), others by angles less than 27°. This is the largest supercluster. The particular solution used for the following analysis was the lowest-energy member of this supercluster, which is 3.5 kcal/mol less favorable than the lowest-energy solution.

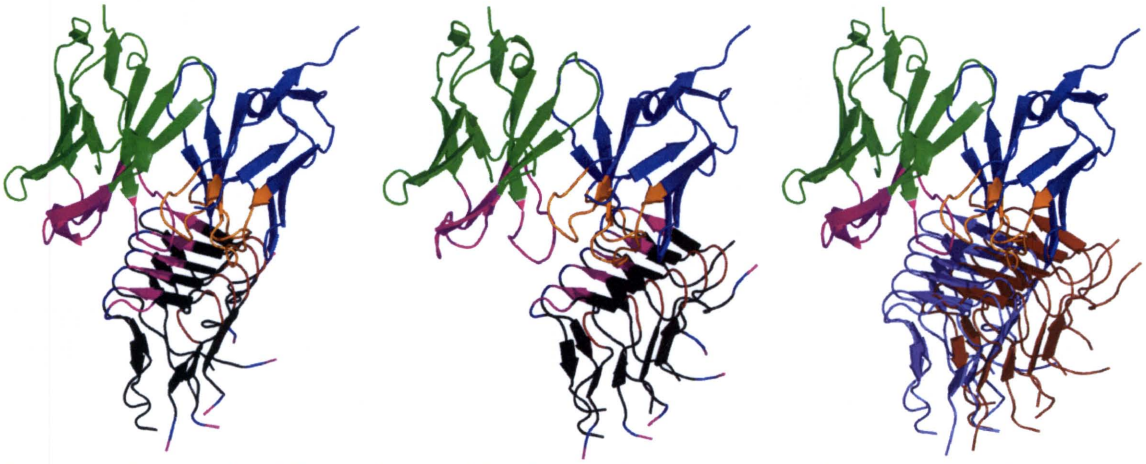

Figure 5. a. WO1 and b. WO2 Fv docked with Aβ6 protofilament model in the predicted configuration. The heavy chain is on the left, the light chain is on the right, and the CDRs are highlighted. The Aβ6 model is shown colored according to residue: negative, red; positive, blue; polar, pink; hydrophobic, black. c. The two solutions are showed overlain.

Salt Bridges and Ion Pairs. This docking model indicates that the line of Glu22 and Asp23 residues in the Aβ6 model binds to the corresponding line of polar and positively charged residues of WO1's light-chain CDR through salt bridges and hydrogen bonds. The line of Lys28 residues likewise interact with the trail of polar and negatively charged residues of the light *and* heavy chain CDRs. Breaking the pairs down by Szilyagi and Zavodsky classification, there are four bonds at < 4.0 Å, six bonds between 4.0 and 6.0 Å, and ten pairs between 6.0 and 8.0 Å.

Hydrogen Bonding. The O and N atoms of the side chains of the line of Asn27 residues on the Aβ6 model make hydrogen bonds with Tyr and Asp residues of WO1. The carbonyl O atoms of the line of (inward-pointing) Val24 and Gly25 residues bond to Tyr residues of WO1. The backbone N of inward-pointing Ser26 makes some possible hydrogen-bonds. There are 17 likely H-bonds at less than 3.5 Å (two of which were also counted as close ion pairs), and 56 possible H-bonds between 3.5 and 5.0 Å (five of which were counted as close or mid-range ion pairs). There is some overlap with the salt bridges listed above.

Hydrophobic Interactions. There are no aromatic rings on the B-face of the Aβ6 model, and the hydrophobic Val24 side chain points toward the interior of the Aβ6 model, so hydrophobic interactions between WO1 and the Aβ6 model are not observed in this docking model.

Docking. WO2-Aβ6. AutoDock3 predicted 50 binding configurations for WO2- Aβ6. Both Abs were treated as rigid bodies. For WO1- Aβ6, Autodock3 found 42 distinct conformational clusters (using an RMSD-tolerance of 1.0 Å), of which 5 contained more than one member. The variation in energy from the best to the worst solution was 9.3 kcal/mol. There was one cluster of two solutions in the top 13, but the largest cluster began with the 14^{th}-ranked solution. Within 1.0 Å R.M.S.D., there are 5 similar solutions. In total, 11 solutions have the B face of the Aβ6 protofilament model at the light-chain CDR, with slight overlap onto heavy chain CDR. One of them is offset by one monomer, others by acute angles. This is the largest supercluster. This solution resembles the supercluster solution found in the WO1 docking, but makes a ~16° angle to it. The particular solution used for the following analysis was the lowest-energy member of this supercluster, which is 6.4 kcal/mol less favorable than the lowest-energy solution.

Salt Bridges and Ion Pairs. The analysis for this docked conformation is very similar to that of the WO1-Aβ6 solution, but there are no salt bridges at less than 4.0 Å, only two ion pairs between 4.0 and 6.0 Å, and five between 6.0 and 8.0 Å.

Hydrogen Bonding. Thirteen likely hydrogen-bonds at less that 3.5 Å and 66 possible hydrogen-bonds between 3.5 and 5.0 Å exist between WO2's Fv model and the docked Aβ6 model.

Hydrophobic Interactions. No hydrophobic interactions were observed for this docking model.

Binding vs. Salt Concentration. Binding was tested under three different ionic strength conditions: 0 mM NaCl, 150 mM NaCl, and 600 mM NaCl (Table 1). Binding was strongest in the near physiological ionic strength buffer, 150 mM NaCl, at an affinity of 4 nM (Figure 6). In a low ionic strength buffer, 5 mM HEPES only, binding is similar. In a high ionic strength buffer, 600 mM NaCl, binding dropped sharply. This manifested in a reduction of both the magnitude and the affinity of binding. 5 mM HEPES only: 4 nM; 150 mM NaCl: 4 nM; 150 mM KCl: 8 nM; 75 mM $NaPO_4$: 10 nM; 600 mM NaCl: 20 nM; and 1xPBS: 2 nM. The significantly reduced binding in high salt suggests that electrostatic interactions are relatively important to binding and hydrophobic interactions are relatively unimportant.

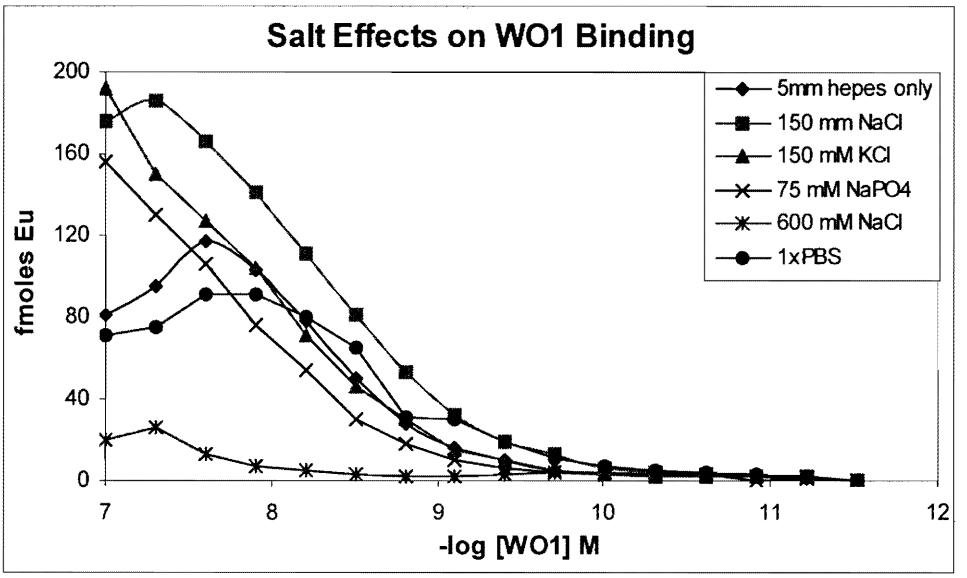

Figure 6. Salt effect on WO1 binding. Binding under various salt conditions was calculated from sigmoid midpoints: 5 mM HEPES only was 4 nM, 150 mM NaCl was 4 nM, 150 mM KCl was 8 nM, 75 mM $NaPO_4$ was 10 nM, 600 mM NaCl was 20 nM, and 1xPBS was 2 nM.

WO1 binding was tested in a range of pH conditions. Citrate pH 3.0 showed essentially no binding, citrate pH 5.8 shows 2 nM binding, PIPES pH 5.8 was > 20 nM, PIPES pH 7.4 was 2 nM, Bicine pH 7.4 was 1.5 nM, Bicine pH 8.5 was 16 nM, CHES pH 8.5 was 10 nM, pH 10.0 > 50 nM). The data produced a continuum of binding affinities with the strongest binding at near physiological conditions, pH 7.4 (Figure 7). There was, however, a discontinuity at pH 5.8 between the PIPES and citrate buffers. Even with the gap present, a clear trend arose with binding dropping off sharply at higher and lower pH conditions. This indicates that WO1 is pH-optimized for Aβ amyloid binding. If hydrophobic interactions were predominant in binding, this would likely not be the case. This reinforces the salt effect results suggesting that binding depends at least in part on electrostatic interactions.

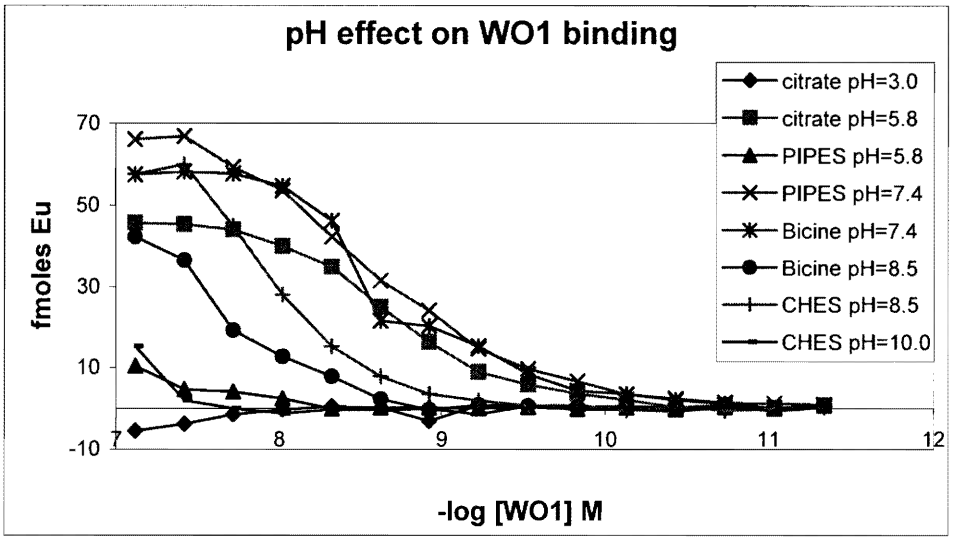

Figure 7. pH effect on WO1 binding. The show binding under various pH conditions. Binding affinities were calculated from the sigmoid midpoints: citrate pH 3.0 showed essentially no binding, pH 5.8 was 2 nM, PIPES pH 5.8 was more than 20 nM, pH 7.4 was 2 nM, Bicine pH 7.4 was 1.5 nM, pH 8.5 was 16 nM, CHES pH 8.5 was 10 nM, pH 10.0 was very low binding (could not be calculated, but no better than 50 nM).

DISCUSSION

Comparison with experimental results. The model of WO1- Aβ6 docking that we have proposed, featuring many H-bonding pairs and salt-bridges, is in agreement with salt-dependence binding studies. It suggests that the positive-negative pattern on the "B" face of the Aβ6 model of the amyloid Aβ protofilament offers a good recognition template for antibodies. The docking model shown in Figure 5(a) is in agreement with the experimental data available on salt effects in WO1- Aβ binding. The bonding of WO2 to the Aβ6 model has no strong salt bridges, which suggests that salt-effects for WO2 and Aβ will be less than those for WO1 and Aβ, and that hydrogen bonds are of paramount importance for WO2-Aβ binding.

Assemblies. Strictly speaking, the Fv models presented here are docked only to a protofilament, but these docked models are consistent with the hierarchical fibril model for Aβ amyloid proposed by Guo, Wetzel, and Ying. Their model consists of six Aβ6 prisms, packed vertically against one another in two rows of three. Our rendering of this model, shown in figure 4,

shows that each protofilament face is exposed twice on the outside surface of the fibril model. The Aβ6 model likewise models a single antigen-recognition region for WO1/WO2, whereas the physiological IgM presents ten recognition sites, resulting in high avidity and increased total binding strength.

Implications. The in-register parallel beta-stacking of the Aβ6 model requires that each residue of the polypeptide line up with its equivalent in the next layer of the prism. Thus, while Glu22 is makes peptide bonds to Ala21 and Asp23, it makes hydrogen bonds to Glu22 on neighboring strands. Viewing a face of the prism, then, one would see lines of equivalent residues. The line of Glu22 and Asp23 residues (Figure 3) is predicted to bind to the corresponding line of positive and polar residues of WO1's light-chain CDR. The line of Asn27 and Lys28 residues likewise interact with the trail of negative and polar residues.

The lineup of positive and negative charges on the B face with those at the CDR suggests another available binding mode. The A face of the Aβ6 model also has such a lineup of charges (Figure 3). The N-terminal residues of the Aβ6 model occlude part of the A face in this model, which was not allowed torsional freedom, so the A face was less accessible for binding than the B face. Even so, 2/50 unclustered solutions for WO1 and 5/50 for WO2 (out of fifty) did predict some form of docking to the A face. It is worth noting, furthermore, that earlier simulations with an un-minimized Aβ6 model (in which the N terminal residues took other orientations) yielded a supercluster of docking solutions at the A face of the Aβ6 model with WO1. It is thus likely that a more computationally intensive docking simulation, one which allowed rotation around the bonds of the Aβ6 model, would have shown a bimodal distribution of solutions, one at the A face and another at the B face. Therefore WO1/WO2 binding to the A face of Aβ remains a distinct possibility.

The C face of the Aβ6 model present mostly hydrophobic residues and positively charged residues and would seem to be a poor fit for the WO1 and WO2 CDRs. Nonetheless, 8/50 unclustered solutions for WO1 and 9/50 for WO1 predicted some form of binding to the C face. While these solutions are unrelated and unclustered, they may have some relevance, so binding Aβ to the C face cannot be ruled out.

Conclusions.

The sequences of two amyloid-recognizing IgMs were compared and analyzed. Structural models of their Fvs were created. WO1's Fv was found to be unusually rich in charged residues, while WO2 is rich in Ser residues. Conditions for simulating the docking of Aβ amyloid protofilament to these Fvs were reported. Autodock3 predicted binding between the protofilament face consisting of residues 23-27 ("B") and the CDRs of the antibodies. The results for WO1 agree with experimental salt-binding data and support a parallel cross-beta model for amyloid protofilament.

Acknowledgments

Juntao Guo and Ying Xu provided the Aβ6 protofilament model. Ms. Kimberly Salone provided high-fidelity sequencing information for WO1 and WO2.

Docking and computational work was done with Dr. Anna Gardberg in the Dealwis lab, who also contributed to and aided in the writing of the docking portions of the paper.

Salt binding assays were performed by Israel Huff in the Wetzel lab, the unpublished data given via communication.

Lab of Chris Dealwis supported through the University of Tennessee at Knoxville, Department of Biochemistry, Cellular and Molecular Biology. Lab of Ron Wetzel supported through the University of Tennessee at Knoxville Graduate School of Medicine.

Grant sponsors: Work for this project supported by NIH grant RO1-1018-84 (Dealwis lab), NIH grant from the NCI, RO1-101-8086 (Chris Dealwis), and NIH grant 5R01NS046356-03.

References

1. Falk RH, Comenzo RL, Skinner M. The systemic amyloidoses. N Engl J Med 1997;337(898-909).
2. Selkoe DJ. Toward a comprehensive theory for Alzheimer's disease. Hypothesis: Alzheimer's disease is caused by the cerebral accumulation and cytotoxicity of amyloid beta-protein. Ann N Y Acad Sci 2000;924:17-25.
3. Tariska I. Alzheimer's fibrillary degeneration in circumscribed cerebral atrophy. Acta Med Acad Sci Hung 1965;21(4):483-495.
4. Temussi PA, Masino L, Pastore A. From Alzheimer to Huntington: why is a structural understanding so difficult? Embo J 2003;22(3):355-361.
5. Jaikaran ET, Clark A. Islet amyloid and type 2 diabetes: from molecular misfolding to islet pathophysiology. Biochim Biophys Acta 2001;1537(3):179-203.
6. Hayden MR, Tyagi SC. "A" is for amylin and amyloid in type 2 diabetes mellitus. Jop 2001;2(4):124-139.
7. Corti O, Brice A. [Parkin, alpha-synuclein and other molecular aspects of Parkinson's disease]. J Soc Biol 2002;196(1):95-10.
8. Kruger R, Eberhardt O, Riess O, Schulz JB. Parkinson's disease: one biochemical pathway to fit all genes? Trends Mol Med 2002;8(5):236-240.
9. George JM. The synucleins. Genome Biol 2002;3(1):REVIEWS3002.
10. Pras M, Prelli F, Franklin EC, Frangione B. Primary Structure of an Amyloid Prealbumin Variant in Familial Polyneuropathy of Jewish Origin. Proc Natl Acad Sci U S A 1983;80(2):539-542.
11. Feiner HD. Pathology of dysproteinemia: light chain amyloidosis, non-amyloid immunoglobulin deposition disease, cryoglobulinemia syndromes, and macroglobulinemia of Waldenstrom. Hum Pathol 1988;19(11):1255-1272.
12. Buxbaum JN, Chuba JV, Hellman GC, Solomon A, Gallo GR. Monoclonal immunoglobulin deposition disease: light chain and light and heavy chain deposition diseases and their relation to light chain amyloidosis. Clinical features, immunopathology, and molecular analysis. Ann Intern Med 1990;112(6):455-464.
13. Bellotti V, Mangione P, Merlini G. Review: Immunoglobulin Light Chain Amyloidosis-The Archetype of Structural and Pathogenic Variability. J Struct Biol 2000;130:280-289.
14. Ross CA. Polyglutamine pathogenesis: emergence of unifying mechanisms for Huntington's disease and related disorders. Neuron 2002;35(5):819-822.
15. Weissmann C. The state of the prion. Nat Rev Microbiol 2004;2(11):861-871.
16. Inouye H, Fraser PE, Kirschner DA. Structure of beta-crystallite assemblies formed by Alzheimer beta-amyloid protein analogues: analysis by x-ray diffraction. Biophys J 1993;64(2):502-519.
17. Sunde M, Blake C. The structure of amyloid fibrils by electron microscopy and X-ray diffraction. Adv Protein Chem 1997;50:123-159.
18. Malinchik SB, Inouye H, Szumowski KE, Kirschner DA. Structural analysis of Alzheimer's beta(1-40) amyloid: protofilament assembly of tubular fibrils. Biophys J 1998;74(1):537-545.
19. Williams AD, Portelius E, Kheterpal I, Guo JT, Cook KD, Xu Y, Wetzel R. Mapping abeta amyloid fibril secondary structure using scanning proline mutagenesis. J Mol Biol 2004;335(3):833-842.

20. Harper JD, Wong SS, Lieber CM, Lansbury PT, Jr. Assembly of A beta amyloid protofibrils: an in vitro model for a possible early event in Alzheimer's disease. Biochemistry 1999;38(28):8972-8980.
21. Serpell LC, Sunde M, Benson MD, Tennent GA, Pepys MB, Fraser PE. The protofilament substructure of amyloid fibrils. J Mol Biol 2000;300(5):1033-1039.
22. Saido TC, Yamao-Harigaya W, Iwatsubo T, Kawashima S. Amino- and carboxyl-terminal heterogeneity of beta-amyloid peptides deposited in human brain. Neurosci Lett 1996;215(3):173-176.
23. Kheterpal I, Williams A, Murphy C, Bledsoe B, Wetzel R. Structural features of the Abeta amyloid fibril elucidated by limited proteolysis. Biochemistry 2001;40(39):11757-11767.
24. Antzutkin ON, Leapman RD, Balbach JJ, Tycko R. Supramolecular structural constraints on Alzheimer's beta-amyloid fibrils from electron microscopy and solid-state nuclear magnetic resonance. Biochemistry 2002;41(51):15436-15450.
25. Torok M, Milton S, Kayed R, Wu P, McIntire T, Glabe CG, Langen R. Structural and dynamic features of Alzheimer's Abeta peptide in amyloid fibrils studied by site-directed spin labeling. J Biol Chem 2002;277(43):40810-40815.
26. Petkova AT, Ishii Y, Balbach JJ, Antzutkin ON, Leapman RD, Delaglio F, Tycko R. A structural model for Alzheimer's beta -amyloid fibrils based on experimental constraints from solid state NMR. Proc Natl Acad Sci U S A 2002;99(26):16742-16747.
27. Burkoth TS, Benzinger TLS, Urban V, Morgan DM, Gregory DM, Thiyagarajan P, Botto RE, Meredith SC, Lynn DG. Structure of the ß-Amyloid (10-35) Fibril. J Am Chem Soc 2000;122:7883-7889.
28. Kheterpal I, Lashuel HA, Hartley DM, Walz T, Lansbury PT, Jr., Wetzel R. Abeta protofibrils possess a stable core structure resistant to hydrogen exchange. Biochemistry 2003;42(48):14092-14098.
29. Wang SS, Tobler SA, Good TA, Fernandez EJ. Hydrogen exchange-mass spectrometry analysis of beta-amyloid peptide structure. Biochemistry 2003;42(31):9507-9514.
30. Kraus M, Bienert M, Krause E. Hydrogen exchange studies on Alzheimer's amyloid-beta peptides by mass spectrometry using matrix-assisted laser desorption/ionization and electrospray ionization. Rapid Commun Mass Spectrom 2003;17(3):222-228.
31. Kheterpal I, Zhou S, Cook KD, Wetzel R. Abeta amyloid fibrils possess a core structure highly resistant to hydrogen exchange. Proc Natl Acad Sci U S A 2000;97(25):13597-13601.
32. Benzinger TL, Gregory DM, Burkoth TS, Miller-Auer H, Lynn DG, Botto RE, Meredith SC. Propagating structure of Alzheimer's beta-amyloid(10-35) is parallel beta-sheet with residues in exact register. Proc Natl Acad Sci U S A 1998;95(23):13407-13412.
33. Perutz MF, Finch JT, Berriman J, Lesk A. Amyloid fibers are water-filled nanotubes. Proc Natl Acad Sci U S A 2002;99(8):5591-5595.
34. Tjernberg LO, Tjernberg A, Bark N, Shi Y, Ruzsicska BP, Bu Z, Thyberg J, Callaway DJ. Assembling amyloid fibrils from designed structures containing a significant amyloid beta-peptide fragment. Biochem J 2002;366(Pt 1):343-351.
35. Hilbich C, Kisters-Woike B, Reed J, Masters CL, Beyreuther K. Aggregation and secondary structure of synthetic amyloid beta A4 peptides of Alzheimer's disease. J Mol Biol 1991;218(1):149-163.
36. Chaney MO, Webster SD, Kuo YM, Roher AE. Molecular modeling of the Abeta1-42 peptide from Alzheimer's disease. Protein Eng 1998;11(9):761-767.

37. Serpell LC, Blake CC, Fraser PE. Molecular structure of a fibrillar Alzheimer's A beta fragment. Biochemistry 2000;39(43):13269-13275.
38. Guo JT, Wetzel R, Xu Y. Molecular modeling of the core of Abeta amyloid fibrils. Proteins 2004;57(2):357-364.
39. O'Nuallain B, Wetzel R. Conformational Abs recognizing a generic amyloid fibril epitope. Proc Natl Acad Sci U S A 2002;99(3):1485-1490.
40. Dumoulin M, Dobson CM. Probing the origins, diagnosis and treatment of amyloid diseases using antibodies. Biochimie 2004;86(9-10):589-600.
41. Whitelegg NR, Rees AR. WAM: an improved algorithm for modelling antibodies on the WEB. Protein Eng 2000;13(12):819-824.
42. Wetzel R, et al. Unpublished communication; 2004.
43. Molecular Operating Environment: Chemical Computing Group Inc.; 1997.
44. Abola EE, Sussman JL, Prilusky J, Manning NO. Protein Data Bank archives of three-dimensional macromolecular structures. Methods Enzymol 1997;277:556-571.
45. Sussman JL, Lin D, Jiang J, Manning NO, Prilusky J, Ritter O, Abola EE. Protein Data Bank (PDB): database of three-dimensional structural information of biological macromolecules. Acta Crystallogr D Biol Crystallogr 1998;54(Pt 6 Pt 1):1078-1084.
46. Martin AC. Accessing the Kabat antibody sequence database by computer. Proteins 1996;25(1):130-133.
47. Altschul SF, Madden TL, Schaffer AA, Zhang J, Zhang Z, Miller W, Lipman DJ. Gapped BLAST and PSI-BLAST: a new generation of protein database search programs. Nucleic Acids Res 1997;25(17):3389-3402.
48. Chothia C, Lesk AM. Canonical structures for the hypervariable regions of immunoglobulins. J Mol Biol 1987;196(4):901-917.
49. Wu TT, Kabat EA. Possible use of similar framework region amino acid sequences between human and mouse immunoglobulins for humanizing mouse antibodies. Mol Immunol 1992;29(9):1141-1146.
50. Martin AC, Cheetham JC, Rees AR. Modeling antibody hypervariable loops: a combined algorithm. Proc Natl Acad Sci U S A 1989;86(23):9268-9272.
51. Martin AC, Cheetham JC, Rees AR. Molecular modeling of antibody combining sites. Methods Enzymol 1991;203:121-153.
52. Rees AR, Searle,S.M.J., Henry,A.H.and Pedersen,J.T. In: M.J.E. S, editor. Protein Structure Prediction. Oxford: Oxford University Press; 1996. p 141–172.
53. Pedersen JT, Searle,S.M.J., Henry,A.H. and Rees,A.R. Immunomethods 1992;1:126.
54. Weiner SJK, P. A.; Case, D. A.; Singh, U. C.; Ghio, C.; Alagona, G.; Profeta, S., Jr.; Weiner, P. J Am Chem Soc 1984; 106:765.
55. Weiner SJK, P. A.; Nguyen, D. T.; Case, D. A. An all atom force field for simulations of proteins and nucleic acids. J Comput Chem 1986;7:230 - 252.
56. InsightII. San Diego: Accelrys; MSI; 2000.
57. Murshudov G. Refinement of macromolecular structures by the maximum-likelihood method. Acta Crystallogr D Biol Crystallogr 1997;53(3):240-255.
58. Collaborative Computational Project N. The CCP4 Suite: Programs for Protein Crystallography. Acta Crystallogr D 1994;50:760-763.
59. Morris GM, Goodsell DS, Halliday RS, Huey R, Hart WE, Belew RK, Olson AJ. Automated docking using a Lamarckian genetic algorithm and an empirical binding free energy function. Journal of Computational Chemistry 1998;19(14):1639-1662.

60. Cole C, Warwicker J. Side-chain conformational entropy at protein-protein interfaces. Protein Sci 2002;11(12):2860-2870.
61. DeLano WL. The PyMOL Molecular Graphics System. San Carlos, CA, USA: DeLano Scientific; 2002.

Appendix 1
IgM Structure and Optimized WO1-WO2 Protelolytic Cleavage

An IgM is a pentameric antibody molecule, with each of the five subunits having IgG-like structure, with two Fab antigen binding sites. A joining, or "J" chain connects the five μ heavy chains. A schematic of this pentameric arrangement is shown below:

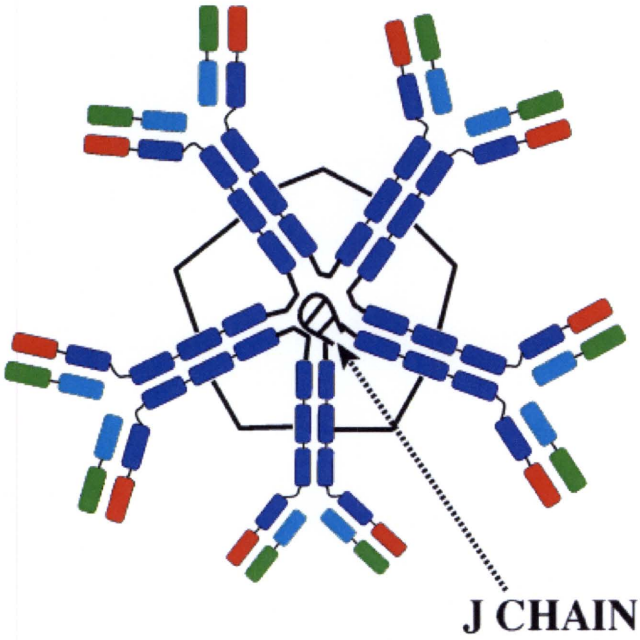

Due to the large size of the IgM (nearly 900kDa), crystallization of the intact Ab is extremely difficult and an IgM structure has not been solved. Thus, efforts have been made to enzymatically fragment the IgM into smaller, more crystallizable protein pieces. Considering the aim of the WO1-WO2 project is to further elucidate amyloid structure, crystallization of the amyloid fibril binding Fab fragment is an obvious goal, with the structure of the CDR regions showing motifs for antigen recognition as well as confirming the docking models. In order to achieve this, a cleavage protocol has been designed an optimized, utilizing the protease papain. A schematic of papain cleavage is shown below:

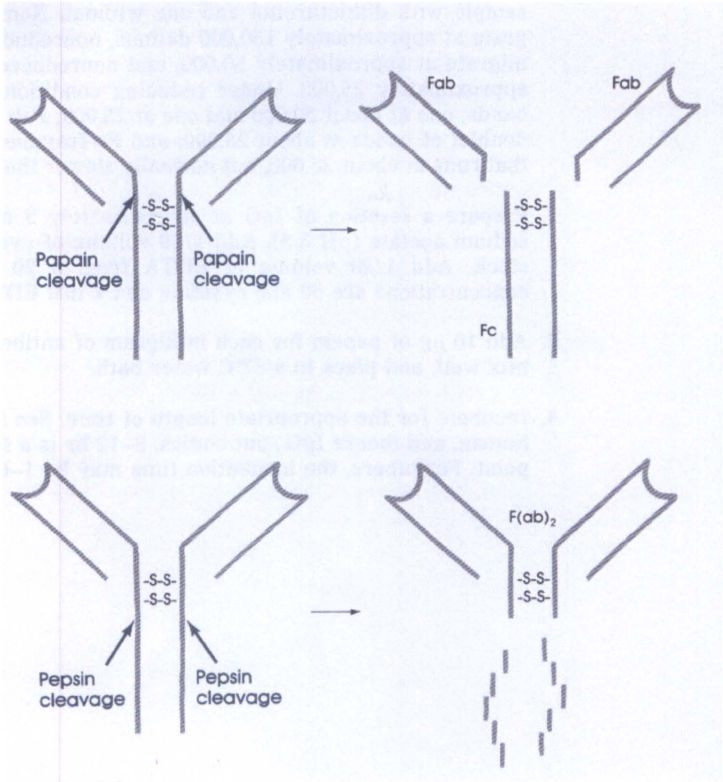

Papain cleaves in the hinge region, just above the two disulfide bonds, resulting in two Fab domains from every IgG. In the case of WO1 and WO2, ten Fab's would be cleaved from the IgM monomer, purified and crystallized. Each IgM is obviously different, so a cleavage protocol should be tailored to the Ab through optimization. Our optimization involved varying pH, papain:Ab ratio, and time, with the procedure as follows:

1. Purify WO1 or WO2 from hybridoma culture through size exclusion chromatography
2. Preactivation of papain in 50mM NaCl, 50mM NaPO4, 10mM cysteine, 2mM EDTA, pH 6,6.5,7 30 minutes at 37°C.
3. Add papain at 1:40 and 1:8 (five fold change) ratios
4. Incubate at 37°C for 12 hours, taking timepoint samples at 30min, 1h, 2h, 4h, 8h, 12h.
5. Run SDS-PAGE gel electrophoresis with Coomassie or silver staining to analyze cleavage
6. Select best conditions, repeat experiment full scale
7.. Purify Fab through affinity or size exclusion chromatography, crystallize.

Our results showed that the pH 7.0, 4hr, 2.5% papain condition shows adequate cleavage with relatively little non-specific cleavage side products. This can be seen on the silver stained SDS PAGE gel below, with our optimal condition seen on the far left, the band in the middle of the image:

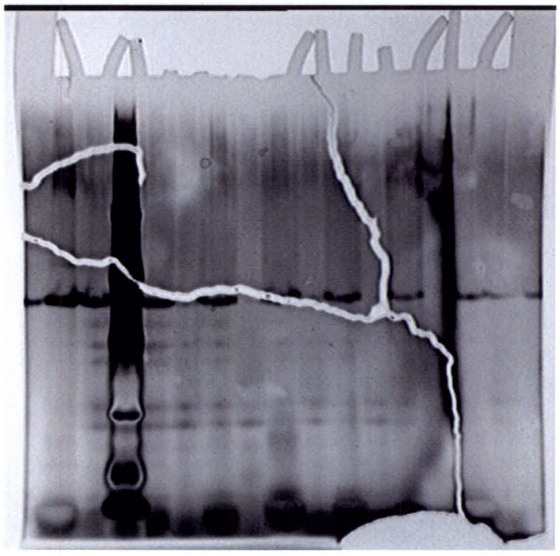

Problems in purification stem from the fact that the Fc regions of the IgM might be cleaved from the J chain, leaving both the Fc and Fab chains at nearly the same molecular weight (~50kDa). Thus size exclusion chromatography may not be efficient, and affinity resins such as Protein L or Protein A columns that bind Fc domains can be employed to purify the Fab.

An image of very small crystals is shown here:

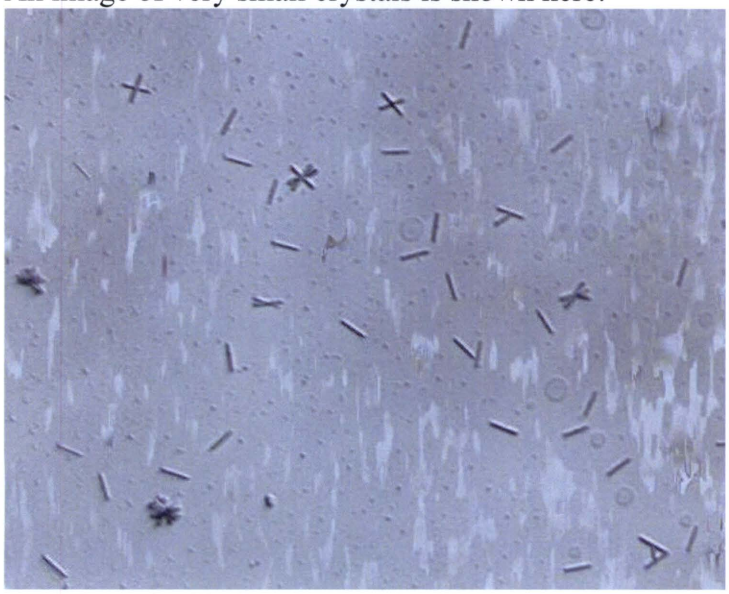

Once these can be optimized, grown to sufficient size, and found to diffract X-rays, a structure of the Fab domains of WO1 and WO2 could be found. This work is ongoing, and a solved structure will contribute substantially to the docking motif proposed.

Appendix 2
WAM generated model images

For reference, several of the WAM generated WO1 and WO2 models rendered using InsightII on a Silicon Graphics Octane™ workstation are shown below:

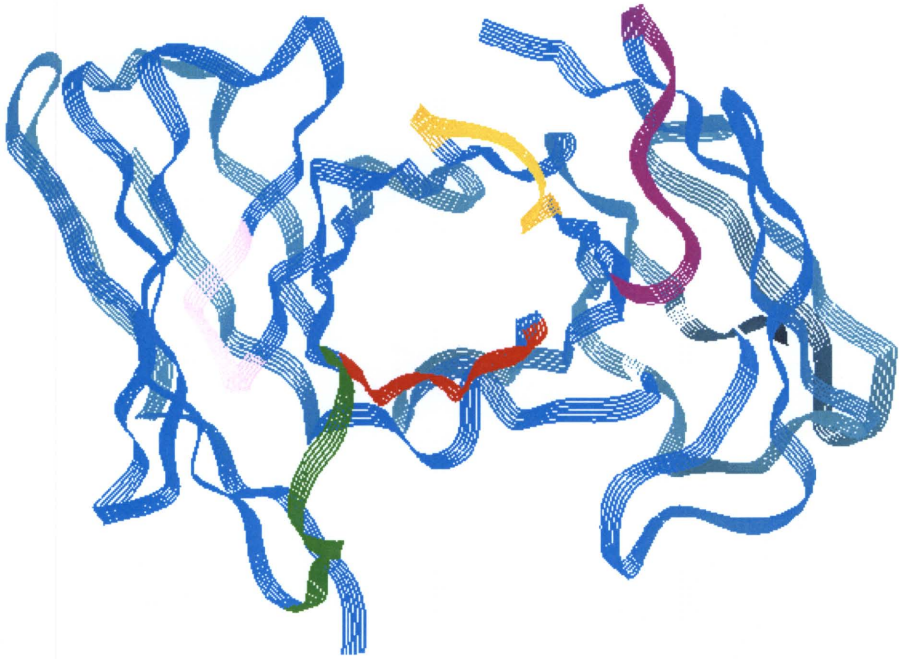

This is a ribbon view of the model of WO2, with heavy chain on left and light chain on the right. CDRs are marked by the colored regions:

pink: Heavy Chain CDR2
green: Heavy Chain CDR1
red: Heavy Chain CDR3
orange: Light Chain CDR2
purple: Light Chain CDR1
white: Light Chain CDR3

Below is a ribbon view of the superimposition of the two models, with similar orientation to the image above, the viewer facing into the Fab CDR region. Obviously, the two share a high degree of structural homology:

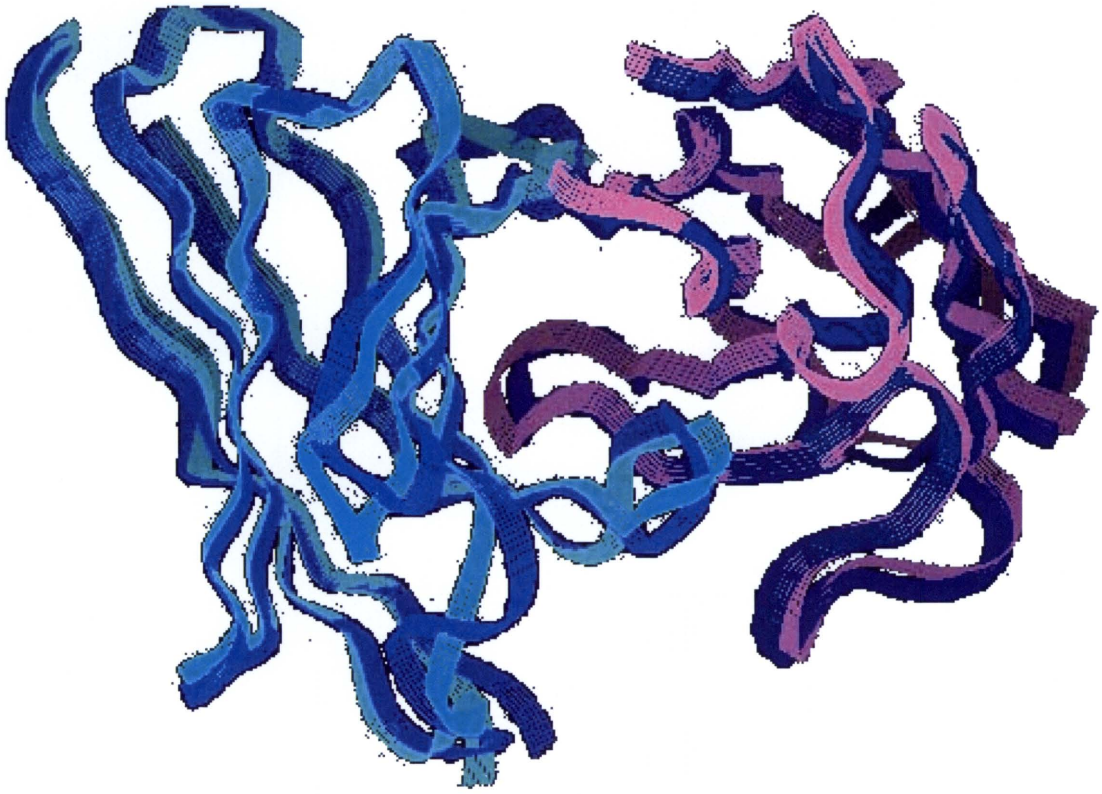

Appendix 3
Electrostatic Surface Images

More detailed images of the DelPhi generated electrostatic surfaces are shown below, viewer looking into the CDRs with heavy chain on left and light on right.

WO1:

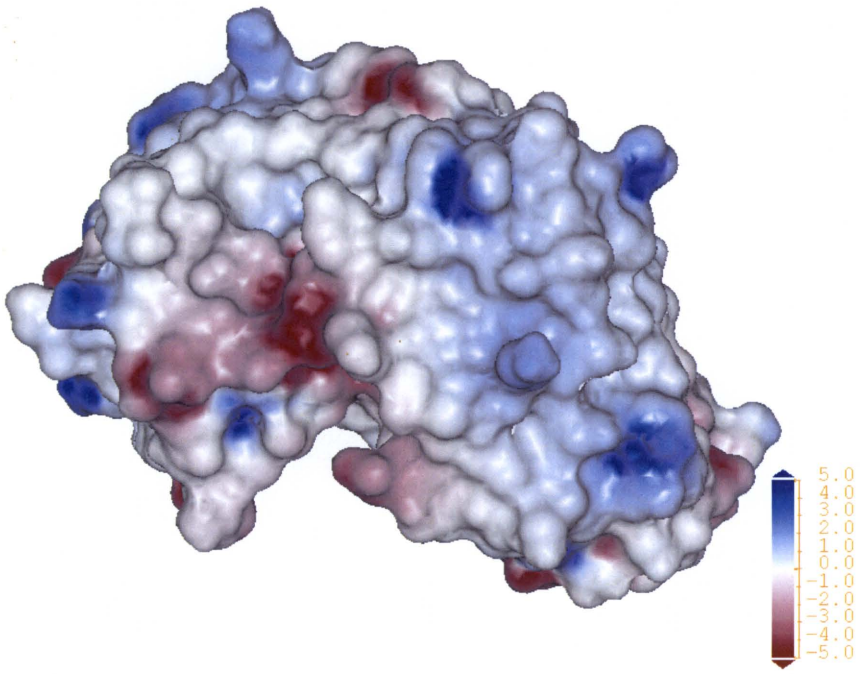

WO2: